



Facile In-Situ Synthesis of Nanocrystalline Celluloses-Silver Bio-nanocomposite for Chitosan Based Active Packaging

Mona T. Al-Shemy^{1*}, Amira M. El-Shafei², Aly Al-Sayed³ and Abeer M. Adel¹



¹ National Research Centre, Cellulose and Paper Department, 33El-Bohouth St. (Former El-Tahrir St.), Dokki, P.O. 12622, Giza, Egypt.

² National Research Centre, Textile Research and Technology Institute, 33El-Bohouth St. (Former El-Tahrir St.), Dokki, P.O. 12622, Giza, Egypt.

³ National Research Centre, Water Pollution Research Department, 33El-Bohouth St. (Former El-Tahrir St.), Dokki, P.O. 12622, Giza, Egypt.

Abstract

In the present study, three different extracted nanocrystalline cellulose (NCs) with different moieties (-COO⁻, SO₄⁻, and PO₄³⁻) were used as both capping and reducing agents for biogenic fabrication of nanocrystalline cellulose-silver (NC-Ag) bio-nanocomposites via a simple, easy and green process. UV-Vis absorption spectra study over a long duration of storage indicates that all colloidal suspensions of the prepared NC-Ag bio-nanocomposites were stable. Disk-diffusion agar method demonstrated various microbial inhibition regions by the three fabricated NC-Ag bio-nanocomposites against four bacterial species: *Bacillus subtilis*, *Escherichia coli*, *Pseudomonas aeruginosa* and *Staphylococcus aureus*. The results obtained by FTIR, UV-visible, XRD, and TEM also indicate the potential effects on the physicochemical properties of chitosan film that occur after loading it with 7% (wt/wt) NC-Ag bio-nanocomposites. Remarkably, the antimicrobial efficacy of the chitosan films differed depending on the films and microorganisms tested. Likewise, the comparison of microbial reduction rates results revealed that Gram-negative bacteria and *Aspergillus niger* fungus were more susceptible to NC-Ag bio-nanocomposites' microbiocidal effects. Thus, these chitosan bio-nanocomposite films can be considered to have broad-spectrum microbiocidal efficacy.

Keywords: Antimicrobial activity; Bio-nanocomposite; Chitosan film; Date palm sheath fibres; Eco-friendly; Nanocrystalline cellulose; silver nanoparticles

1. Introduction

Silver nanoparticles (AgNPs) are the most popular commercial metallic nanoparticles. Because of the widespread anti-microbial activity known since ancient times, silver has been exploited against various organisms such as bacteria, fungi, and viruses [1–3]. Accordingly, the main concerns of active materials developers were their strong antibacterial activity at low concentrations and their stability in severe conditions of temperature and pressure [4, 5]. Many chemical reduction approaches have been used to fabricate AgNPs from silver salts. These methods vary in many aspects such as reducing agent, capping factor, pH, reaction duration, temperature, concentrations, and relative quantities of reagents. Consequently, formed AgNPs vary in diameters, and colors, ranging from yellow to brown [6]. Previous work successfully removed the defects associated

with the chemical synthesis of AgNPs by replacing sodium borohydride, ascorbic acid, citrate and elemental hydrogen reagents with naturally occurring biocompatible substances. In general, plants - specially agricultural residues or wastes- and their extracts provide a typical platform for the fabrications of biogenic AgNPs, because they fulfill scientists' goals of lack of toxicity, eco-friendly, safer, easier and milder synthesis processes [7–11].

Cellulose with abundant reducing hydroxyl groups is a superior candidate for the function of fabricating AgNPs. Various types of cellulose are available for this purpose, such as cellulose microsphere, bacterial cellulose, and various functional cellulose derivatives. Although these types of cellulose have a similar molecular and chemical structure, they show various mechanical and physical

*Corresponding author e-mail: mt.el-shemy@nrc.sci.eg; mona.alshely@yaho.com; mona.alshely@gmail.com.

Receive Date: 07 July 2022, Revise Date: 10 August 2022, Accept Date: 17 August 2022, First Publish Date: 17 August 2022
DOI: 10.21608/EJCHEM.2022.149568.6465

©2023 National Information and Documentation Center (NIDOC)

properties that allow them to be customized for definite implementations.

For example, bringing in new functions in cellulose derivatives enhances their ability to stabilize the nanoparticle attachment [12]. Among the most frequently used chemical modifications of cellulose are etherification, esterification, oxidation, and silanization reactions. Esterification reactions can occur as a side reaction during the use of mineral acids such as sulfuric acid and phosphoric acid in the hydrolysis of amorphous regions of cellulosic materials to extract nanocrystalline cellulose (NC). The sulfate and phosphate groups likely enter the most reactive C6 followed by C2 and C3 finally [13].

Another modification process for cellulose is oxidation with ammonium persulfate (APS). Despite being one of several oxidation protocols, APS has been studied extensively by scientists for being a simpler, greener, and less expensive process that includes extraction of nanocellulose and primary C6-OH oxidation to a carboxyl group [14, 15]. In such cases, besides the anchoring power of nanoparticles, NC possess special properties capable of enhancing the matrix of advanced bio-nanocomposites [16].

Several protocols were proposed related to the fabrication of nanocrystalline cellulose-silver (NC-Ag) bio-nanocomposite. One of these protocols blends NC and AgNPs into a poly (lactic acid) matrix to prepare multifunctional bio-nanocomposites [17]. Others used NC, after activating their fiber surface by TEMPO oxidation reaction, as a capping agent for AgNPs while reducing it with sodium citrate or sodium borohydride [18]. Recently, NCs were utilized as both the capping and the dispersant of AgNPs fabricated using glucose as the reducing agent [19]. Another recently published study used a green photochemical approach to synthesize NC-Ag bio-nanocomposites [20]. However, studies on biogenic synthesis of AgNPs using different modified NC fibers that can act as both a capping and a reducing agent are still insufficient.

The high appeal of packaging materials in the rapidly growing sectors (foodstuffs, cosmetics, toys, tools, chemical drugs, household items ... etc.) has caused a rapid development to replace synthetic packaging materials with new biodegradable ones. Unlike petroleum derivatives-based packaging, the most important advantages of environmentally friendly packaging are safety, biodegradability, and low cost [21]. In this regard, composite materials reinforced with renewable and biodegradable polymers (e.g. cellulose, chitosan, starch, gelatin, alginate...etc.) have been developed to obtain the next generation of sustainable and green materials in the packaging fields [21–23].

Currently, chitosan (CS) based films have been developed as sustainable packing materials due to its availability, biodegradability, antibacterial and antioxidant activities. Moreover, the need for

multifunctional packaging (e.g. antimicrobial, barrier, transparency and mechanical) can be reached via multiple chitosan bio-composite systems formations [24–26]. Several studies have been done to improve the packaging material based on chitosan films by composing them with other active biopolymers such as cellulose, which has valuable advantages such as abundance, renewal, biodegradation and biocompatibility. However, due to the increase in the deficiency of woody biomaterials, much effort is made to find the material that replaces it and which is more available and cheaper such as agricultural residues [27, 28].

To the most of our knowledge, there are no prior studies discussing the influence of functional groups of NCs on the properties of NC-Ag bio-nanocomposites. Hence our first aim was to extract NCs, with different functional moieties (-COO⁻, SO₄⁻, and PO₄⁻), from the agricultural residue of the date palm sheath fibers via hydrolysis with APS, sulfuric acid and phosphoric acid. Accordingly, the AgNPs anchoring sites were established along the NC fibers through oxidation and esterification processes. While the large surface area and high suspension capacity of NC whiskers enhance nucleation of the monodisperse Ag atoms and prohibit their agglomeration. Hence, thanks to the combined benefits of the physical and chemical structure, hydroxyl groups and moieties, NCs can play a triple role as a reducing, capping and dispersant agent for the synthesis of NC-Ag bio-nanocomposites in a simple, easy and green process. The impact of functionalized NCs on permanence and antimicrobial behaviors for in-situ synthesized NC-Ag bio-nanocomposites was investigated too. Thereafter, the fabricated NC-Ag bio-nanocomposites were utilized to modify the main features of chitosan films such as mechanical strength, water vapor barrier, and antimicrobial activities for active packaging applications.

2. Experimental

2.1. Materials

All chemicals used in this study are of chemical grades and used as provided without any further purification. Silver nitrate (PanReac AppliChem) was purchased from Lennox Laboratory Supplies Dublin. Chitosan low molecular weight and ammonium persulfate were obtained from Sigma-Aldrich. Phosphoric (85%) and sulfuric (97%) acids were acquired from Honeywell Specialty Chemicals (Seelze GmbH) and AbcoChemie (ENG. Ltd), respectively. Pulp and bleached pulp were extracted from date palm sheath fibres as previously reported [14].

2.1.1. Preparations of functionalized nanocrystalline celluloses

The three functionalized nanocrystalline celluloses (NCs) used in this work, oxidized nanocellulose; ONC ($-\text{COO}^-$), sulfated nanocellulose; SNC ($-\text{SO}_4^-$) and phosphorylated nanocellulose; PNC ($-\text{PO}_4^{3-}$), were prepared through ammonium persulfate, sulphuric acid and phosphoric acid hydrolysis of pulp and bleached date palm sheath fibres according to our previous works [13, 14, 29]. Scheme 1 summarized the extraction conditions. To extract NCs in brief, the fibers of unbleached pulp (precursor of ONCs) and bleached pulp (precursor of SNC and PNC) were ground in a mill. Then one gram from each was added to a specific concentration of 1.25 M ammonium persulphate, 6.5 M sulfuric acid, and 10.7 M phosphoric acid at 60, 50, and 90 °C for 16, 1.45, and 0.5 h, respectively. At the end of each reaction time, the reaction was terminated by pouring the suspension into ten-fold of iced distilled water and the resultant suspension were dialyzed against bi-distilled water to a pH \approx 6. The final suspensions of functionalized NCs (ONC, SNC, and PNC) were then lyophilized for further characterization and application purposes.

2.1.2. Preparation of nanocrystalline cellulose-silver bio-nanocomposites

In a 250 mL beaker, 1 g of lyophilized ONC was suspended in a certain volume of distilled water (bearing in mind that the total amount of reaction medium was 100 mL) using an ultrasonic water bath (power 1000 W) for 10 min, after which, sodium hydroxide solution (0.25 g/mol) was added dropwise to the ONC suspension with magnetic stirring until reaching pH 10. Next, 5.5 mL of 0.029 g/mol silver nitrate solution was added about one drop per second to the preheated ONC suspension at 55 °C with continued strong stirring. After adding 2 mL of silver nitrate solution, the white ONC suspension turned light yellow. When all the silver nitrate solution was added, the oxidized nanocrystalline cellulose-silver (ONC-Ag) bio-nanocomposites suspension gained reddish-yellow color. The same concentration of silver nitrate (5.5 mL of 0.029 g/mol AgNO_3) was applied to all NC samples (ONC, SNC, and PNC) with the same amount of NC (1 g). The entire addition took about 2 minutes, after which the stirring was stopped and the stir bar was removed. NC-Ag bio-nanocomposites (NC: ONC, SNC, or PNC) prepared from the three different NC moieties ($-\text{COO}^-$, SO_4^- , and PO_4^{3-}), acquired different hues of reddish-yellow, red-brown, and golden-yellow, respectively (as can be seen in Fig. 1a). The three prepared NC-Ag bio-nanocomposites were stable at room temperature and stored in vials at 5 °C for several months.

2.1.3. Preparation of chitosan bio-nanocomposite films

The chitosan bio-nanocomposite films were prepared by mixing 50 mL of 2% chitosan solution (dissolved in 1% acetic acid) with 7% NC-Ag bio-nanocomposites (NC: ONC, SNC or PNC) (wt/wt_{CS}). The bio-nanocomposite mixture was homogenized at 13,500 rpm for 5 min, followed by addition 30% of glycerol plasticizer (wt/wt_{CS}) and stirred for 1 h at 50 °C. After this, the mixture is degassed, poured into Teflon plates, and left to dry in a ventilated oven at 40 °C for 24 h. Dry films were peeled off at an average thickness of 78 μm from the plates and conditioned for 48 h at RH \approx 50 and 25 °C.

2.2. Characterization

2.2.1. FTIR spectroscopy analysis

JASCO FT-IR 6100 spectrometer (Tokyo, Japan) was used to record the FTIR spectra of the differently prepared samples. The measurements were carried out within the range of 4000–400 cm^{-1} , with 60 scans and a resolution of 4 cm^{-1} .

2.2.2. X-ray diffraction (XRD) analysis

Panalytical Empyrean X-ray diffractometer (PANalytical, Netherlands), with an angle of incident monochromatic X-ray in the range of $2\theta=5-80^\circ$, was used to analyze the lyophilized NCs and NC-Ag bio-nanocomposites samples and dry films of chitosan bio-nanocomposite under investigation.

2.2.3. Morphological analysis

Quanta FEG-250 (Waltham, MA, USA) scanning electron microscope, at a voltage of 20 kV, was used for imaging and elemental analysis, by energy-dispersive X-ray spectroscopy, of the films. The transmission electron micrographs of NCs and NC-Ag bio-nanocomposites were captured with high resolution JEOL JEM-2100 (Japan). The ONC, SNC, and PNC suspensions were dried on a microgrid covered with a thin carbon film (\approx 200 nm). In order to enhance the microscopic resolution, the precipitated ONC, SNC, and PNC were dyed with a 2% uranyl acetate solution. On the other hand, the precipitated ONC-Ag, SNC-Ag, and PNC-Ag bio-nanocomposites were left without dyeing.

2.2.4. UV-Vis spectroscopy

The surface plasmon resonance of ONC-Ag, SNC-Ag, and PNC-Ag bio-nanocomposites was characterized by UV-Vis spectroscopy using Agilent's Cary 50 Probe equipment.

2.2.5. Mechanical test for chitosan bio-nanocomposite films

LLOYD LR10k universal testing machine (England) was used to test the mechanical strength properties of films under study. Samples were cut into rectangular shapes with dimensions 15 mm wide

and 70 mm long. Moving clamp speed was set at 10 mm min⁻¹ and gauge length was fixed at 20 mm. Results are the average reading of at least five samples.

2.2.6. Water vapor permeability tests for chitosan bio-nanocomposite films

Water vapor permeability (WVP) was determined according to ASTM E96-E80 using saturated NaCl solution at 25 °C. The results are the average reading of three repeated tests.

2.2.7. Antimicrobial test

Antibacterial tests for NC-Ag bio-nanocomposites suspensions and chitosan bio-nanocomposite films under study were qualitatively performed against four different bacterial species (*Bacillus subtilis* and *Staphylococcus aureus* as gram-positive and *Escherichia coli* and *Pseudomonas aeruginosa* as gram-negative), by disk-diffusion agar method according to AATCC Test Method 147–1988. The qualitative test was carried out using solid media (LB agar) [30]. For NC-Ag bio-nanocomposites suspensions, blank paper disks (Schleicher & Schuell, Spain) with a diameter of 10 mm were steeped in 10 μL of tested suspension (at dilution of 1:20) and placed on LB agar, previously inoculated with the bacteria. While in case of chitosan bio-nanocomposite, films were cut into circular disks with 10 mm diameter and put directly over LB agar. After 48h, the corresponding inhibition zones are measured using slipping calipers of the National Committee for Clinical Laboratory Standards [30].

The chitosan bio-nanocomposite films were also quantified for antimicrobial activity against four different bacterial species (*Bacillus subtilis* and *Staphylococcus aureus* as gram-positive and *Escherichia coli* and *Pseudomonas aeruginosa* as gram-negative), fungi (*Aspergillus niger*) and yeast (*Candida albicans*). Quantitative tests were performed using liquid media (LB Broth). All tubes were injected with 100 μL of microbial suspension and evaluated for antimicrobial activity by adding 100 mg of film. Subsequently, it was incubated in a shaking incubator at 37 °C for 24 h, after which microbial growth was measured by taking the optical density at 600 nm. In order to compare the inhibitory effect of chitosan bio-nanocomposite films with different prepared NC-Ag bio-nanocomposites on culture growth, the results are expressed as a percentage of growth inhibition as shown below [31].

Percentage growth inhibition

$$= \frac{\text{OD of control}}{\text{OD of control} - \text{OD of test}} \times 100$$

2.2.8. Statistical analysis

Results were expressed as the mean of three separate tests, unless otherwise indicated.

3. Results and discussion

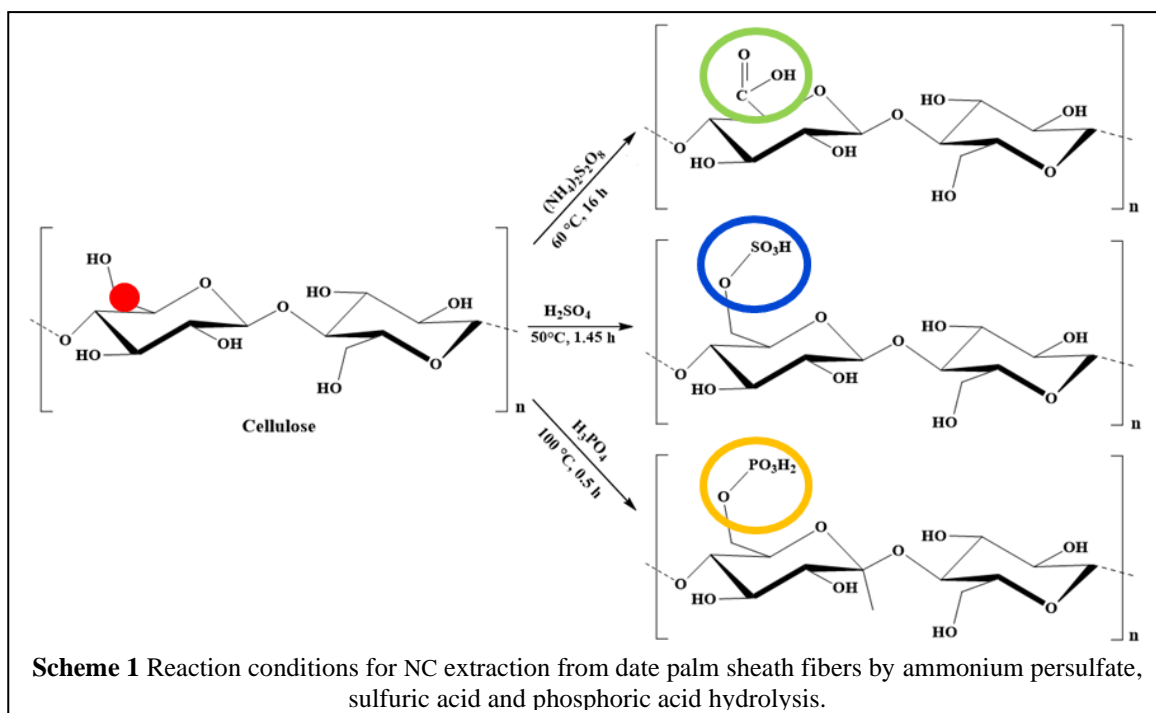
3.1. Mechanism for the biogenic fabrication of NC-Ag bio-nanocomposites

NCs, extracted from date palm sheath fibers, could be a superior template for AgNPs biosynthesis due to their ability to halt the growth of nanoparticles, resulting from the intramolecular and intermolecular hydrogen bond structure. Also, with three reducing hydroxyl groups per anhydroglucose unit and new ionic moieties (i.e. COO⁻, SO₄⁻ and PO₄⁻); thus NCs possess several anchor points for attachments of AgNPs. Concerning the three extracted NCs (ONC, SNC, and PNC), the total charge densities of the carboxylate, sulfate, and phosphate groups on the NC surface, as measured using conductometric titration described in the standard procedure (SCAN-CM 65:02) [32], were found to be 1367, 1433 and 1354 μmol/g for ONC, SNC, and PNC, respectively.

Based on the previously mentioned capacities of NCs in forming AgNPs, we can suggest the following mechanism (Scheme 2). Firstly, an ion-exchange interaction occurs between Na⁺ attached to the active moieties on the surface of cellulose fibers, and Ag⁺ ions. Secondly, a portion of Ag⁺ is reduced to Ag⁰ by the available reducing groups on the surface of NCs. These Ag⁰ atoms act as nucleation centers and stimulate the remaining Ag⁺ reduction in the bulk solution. Then, metal clusters are formed by the polymerization of the atoms due to coalescence. The process continues until larger particles with high nuclearity are formed. Finally, the propagation process is stabilized and terminated by the interaction with cellulose polymer [33, 34].

3.2. UV-Vis spectroscopy analysis

The successful fabrication of NC-Ag bio-nanocomposites using NCs can be verified via several analytical tools. Among them, UV-Vis absorption spectroscopy is one of the most important techniques for determining the synthesis and stability of NC-Ag bio-nanocomposites in aqueous dispersion. Fig. 1a shows the UV absorption spectra and the aqueous suspensions photo of ONC-Ag, SNC-Ag, and PNC-Ag bio-nanocomposites. ONC-Ag, SNC-Ag, and PNC-Ag bio-nanocomposites prepared from three different groups of NC (COO⁻, SO₄⁻ and PO₄⁻) acquired uneven colors ranging from reddish-yellow to red-brown and golden-yellow, respectively. This color difference is attributed to the surface plasmon resonance (SPR) phenomenon of the AgNPs [35, 36]. The successful formation of ONC-Ag, SNC-Ag, and PNC-Ag bio-nanocomposites was inferred by the appearance of a sharp absorption peak, distinctive to SPR of AgNPs, at ≈408 nm with a peak width at half-maximum (PWHM) ranged between 83.38 and 128.80 nm. The values found for the wavelength of plasmon maxima (λ_{max}) and PWHM of fabricated ONC-Ag, SNC-Ag, and PNC-Ag bio-nanocomposites are listed in Table 1.



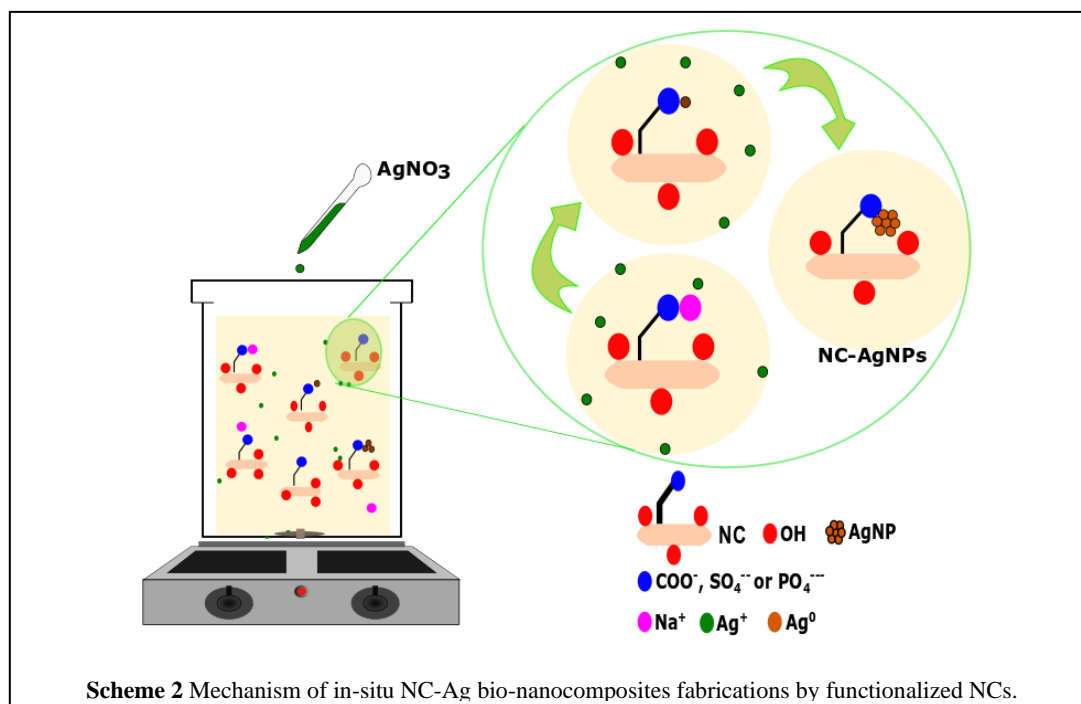
The absorption spectra of ONC-Ag, SNC-Ag, and PNC-Ag bio-nanocomposites with different wavelengths and PWHM illustrate the potential effect of the ONC, SNC, and PNC functional groups of COO^- , SO_4^- and PO_4^{2-} , respectively on the characteristics of ONC-Ag, SNC-Ag, and PNC-Ag bio-nanocomposites.

The phenomenon of dissimilar spontaneous growth and/or agglomeration in AgNPs can strongly influence the stability of their suspension and deteriorate their unique properties, which limit their widespread fields of function. Hence, the stability of ONC-Ag, SNC-Ag, and PNC-Ag bio-nanocomposites in suspensions was monitored after 1, 2, 3 and 5 months using UV-Vis absorption spectroscopy. As can we see from Fig. 1 (b, c, and d), the SPR absorption of the three NC-Ag bio-nanocomposites follows different pathways during storage periods. While SNC-Ag and PNC-Ag continue to grow over time accompanied by an increase in peak intensity, some ONC-Ag accumulates, resulting in a slight decrease in absorption intensity. The relationship between λ_{max} and PWHM for ONC-Ag, SNC-Ag, and PNC-Ag bio-nanocomposites during storage can be better understood by Fig. 1e. λ_{max} of ONC-Ag bio-nanocomposites increases linearly after one month during storage time while PWHM remains constant.

λ_{max} of SNC-Ag bio-nanocomposites follows a different path, the absorption intensity increases first then after one month it reaches steady state, while PWHM reaches a constant width after three months of storage. Unlike ONC-Ag and SNC-Ag bio-nanocomposites, the PWHM of PNC-Ag bio-nanocomposites decreases during storage while λ_{max} shifts to a higher wavelength initially and then reaches steady state before rising again after three months. Although such changes occurred, radiation damping still minimal and the size of the plasmon peak did not change significantly, thus the ONC-Ag, SNC-Ag, and PNC-Ag bio-nanocomposites suspensions can be considered stable for more than five months.

Table 1 TEM, UV-Vis and XRD data of ONC-Ag, SNC-Ag, and PNC-Ag bio-nanocomposites

Sample	ONC-Ag	SNC-Ag	PNC-Ag
Av. diameter (nm)	9.01	6.56	14.09
PWHM (nm)	83.38	103.78	128.80
λ_{max} (nm)	406.00	414.00	408.00
Cr.I (%)	81.00	83.50	88.00
Position-2 θ (°)	NC 22.65 Ag 38.07	22.61 38.17	22.53 38.07
d ₂₀₀ -spacing (Å)	NC 3.92 Ag 2.36	3.93 2.35	3.94 2.36
L ₂₀₀ (nm)	NC 6.39 Ag 4.09	7.67 5.49	7.47 6.48



3.3. TEM analysis

Fig. 2 displays TEM micrographs of NCs isolated from the date palm sheath fibers, and their analogs bio-nanocomposites with AgNPs. The prepared ONC, SNC, and PNC exhibited uniform rod-like whiskers with narrow size distributions. Among the three extracted NCs, SNCs exhibited the smallest length and diameter when compared to ONCs and PNCs. On another hand, ONC-Ag, SNC-Ag, and PNC-Ag bio-nanocomposites display a semi-spherical shape and relatively wide size distribution with distinct diameters (as was found from TEM analysis) ranging from 5.56 to 16.67 nm, 4.39 to 10.53 nm, and 7.9 to 21.05 nm for ONC-Ag, SNC-Ag and PNC-Ag, respectively (Fig. 2). The difference between the ONC-Ag, SNC-Ag, and PNC-Ag bio-nanocomposites sizes can be attributed to the physicochemical differences between the three main NCs. The strong intra and intermolecular hydrogen bonding existed in these NCs fibers create a three-dimensional mold structure for fabrication of ONC-Ag, SNC-Ag and PNC-Ag bio-nanocomposites. Fig. 2 also shows the electron diffraction of a selected area (SAED) corresponding to the NC-Ag bio-nanocomposites. One can notice concentric rings with some splashes of diffractions spread around its circumference. These pattern circles are compatible with the cubic Ag structure of (111), (200), (220), (311), (222), (400) and (331) planes [37].

3.4. FTIR analysis

When comparing FTIR spectra of NCs and these for NC-Ag bio-nanocomposites, FTIR spectra exhibited the same spectral features with different intensities and shifted frequencies (Fig. 3). These variations in intensities and positions of the absorption bands can be attributed to the creation of metal-polymer bonds. The following facts can be drawn from this comparison: The absorption peaks corresponding to intra and intermolecular hydrogen bonds stretching of -OH at 3401, 3414 and 3417 cm^{-1} for ONC, SNC and PNC shift to 3420, 3419 and 3425 cm^{-1} for ONC-Ag, SNC-Ag, and PNC-Ag bio-nanocomposites, respectively. This shift in absorption maxima to a higher frequency indicates the bond of free -OHs to Ag. The appearance of new bands ascribed to $\nu(\text{Ag-O})$ in the far IR spectrum at 561; 521, 565; 525 and 564; 522 cm^{-1} for ONC-Ag, SNC-Ag, and PNC-Ag bio-nanocomposites [denoted by the blue arrows], respectively support this idea [38]. Also, alterations of hydrogen bond energy and length of NCs after AgNPs attachment indicate their possible impact on the hydrogen bonds of NCs (Table 2).

The fact that AgNPs have become the most commercialized nanomaterial along with the many benefits of NC can be used to enhance the properties of biodegradable chitosan films. In order to study the effect of NC-Ag bio-nanocomposites on the properties of chitosan films, the chitosan matrix was mixed with 7% NC-Ag bio-nanocomposites.

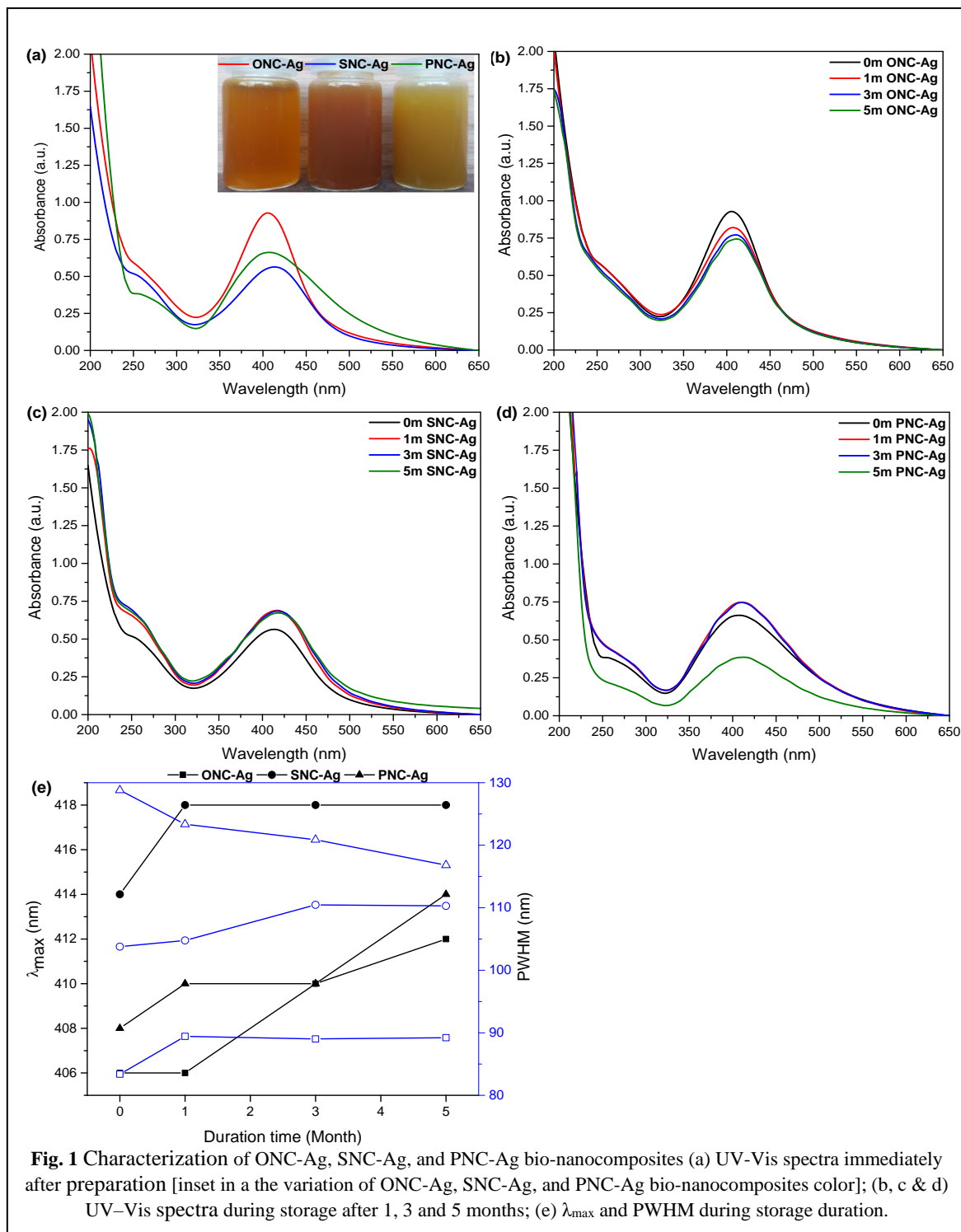
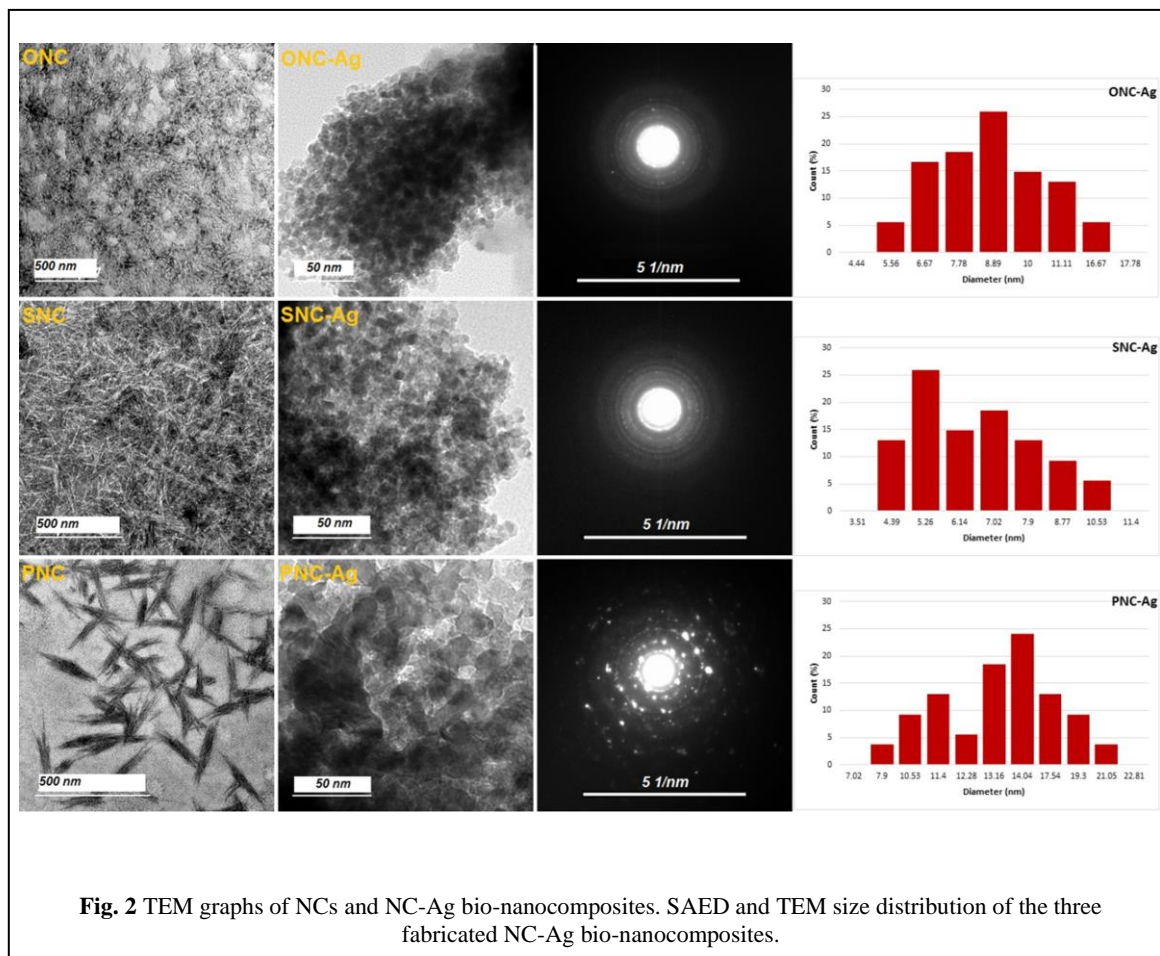


Fig. 4 (a and b) shows the FTIR spectra of the neat chitosan and CS/NC-Ag bio-nanocomposite films. All films manifest the main symmetrical peaks of neat chitosan film with significant changes in intensity. The massive improvement of broadband absorption between 3800–3000 cm^{-1} , due to the coincided vibrations of νNH and νOH from chitosan, can be attributed to the hydrogen bonding network among molecules formed between the available $-\text{OH}$

groups of NC and $-\text{NH}_2$ groups from chitosan [15, 50]. Moreover, spectra of the prepared films revealed two peaks at 2956 and 2890 cm^{-1} , which are due to asym and sym νCH_2 , respectively. Likewise, the corresponding absorption peaks for the amide I ($\nu\text{C}=\text{O}$, νNH), the amide II (δNH , $\nu\text{C}-\text{N}$, $\nu\text{C}-\text{C}$) and amide III ($\nu\text{C}-\text{N}$, δNH) from neat chitosan film appeared at frequencies of 1664, 1598 and 1335 cm^{-1} , respectively.



Once the bio-nanocomposite is formed, the intensity of amide I absorption rises due to the participation of more free -NH_2 groups in the bonding. The growth of peak absorption present at 1444 cm^{-1} , when loading the chitosan matrix with NC-Ag bio-nanocomposites, is an indication of enhanced film crystallinity. This idea is well supported by the disappearance of the amorphous peak at 817 cm^{-1} compared to neat chitosan film [15, 37].

3.5. XRD analysis

XRD diffractograms of ONC-Ag, SNC-Ag, and PNC-Ag bio-nanocomposites, shown in Fig. 5, reflect the diffraction peaks of cellulose I allomorph and cubic AgNPs [20, 38]. The appearance of the characteristic peaks of genuine NCs (Online Resource 1) in ONC-Ag, SNC-Ag, and PNC-Ag bio-nanocomposites at $2\theta \approx 14.97^\circ$ ($\bar{1}\bar{1}\bar{0}$), 16.45° (110), 22.65° (200) and 34.27° (004) indicates that the crystal core of NC whiskers is neither altered nor disordered by the introduction of AgNPs. In addition, the ONC-Ag, SNC-Ag, and PNC-Ag bio-nanocomposites showed additional diffraction peaks located at $2\theta \approx 38.12^\circ$ and 44.31° indexed for Ag (111) and (200) planes (Reference code 04-004-

6434). Segal, Scherrer and Bragg's formulas were used for calculating the crystallinity index (CrI , %), crystallite size (L_{200} , nm) and interplanar spacing (d_{200} -spacing, Å), respectively [44, 51, 52]. The data obtained from XRD are given in Table 1. Likewise, one can get a better perception of compatibility between the crystalline structures of chitosan and NC-Ag bio-nanocomposites from X-ray diffraction patterns of the neat chitosan and chitosan bio-nanocomposite films. Table 3 and Fig. 6 display the changes associated with incorporating chitosan films with NC-Ag bio-nanocomposites. In contrast to the diffractogram of neat chitosan film, the corresponding diffraction peaks of chitosan bio-nanocomposite films appeared at a lower $2\theta^\circ$ position with higher intensity and longer interplanar spacing among lattice planes (d-spacing, Å).

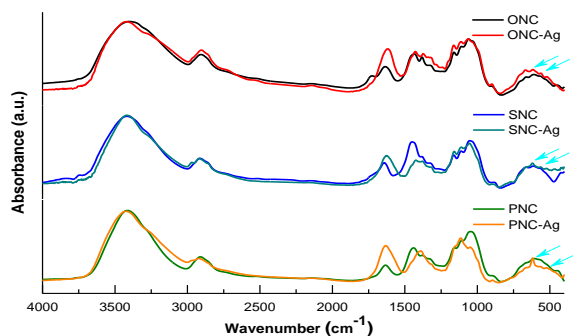


Fig. 3 FTIR spectra of the three extracted NCs and their corresponding biogenic AgNPs.

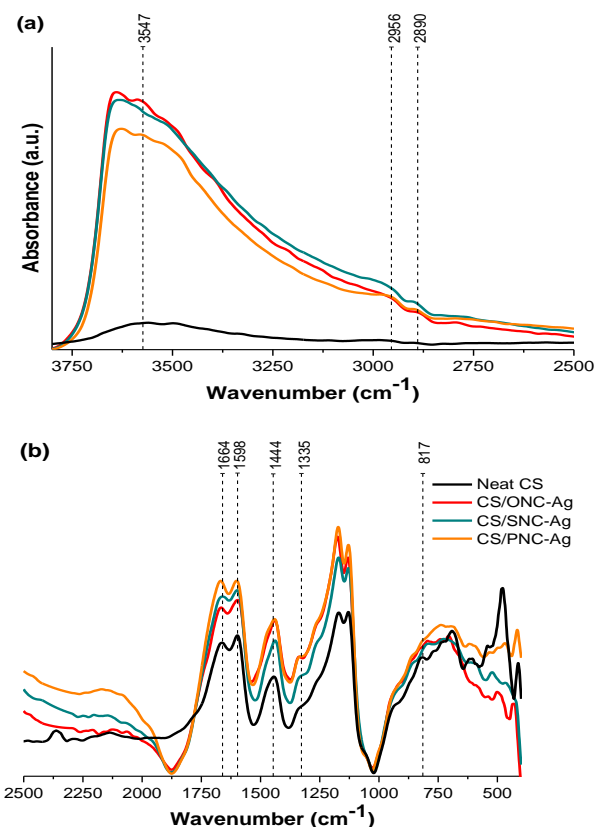


Fig. 4 FTIR spectra of neat chitosan and chitosan bio-nanocomposite films loaded with NC-Ag bio-nanocomposites in the spectral range (a) 3800-2500 cm^{-1} and (b) 2500-500 cm^{-1} .

New crystalline peaks similar to these in XRD patterns of ONC-Ag, SNC-Ag, and PNC-Ag bio-nanocomposites appeared in XRD of CS/ONC-Ag, CS/SNC-Ag and CS/PNC-Ag bio-nanocomposite films at $2\theta = 11.29, 22.66; 11.33, 22.83; 11.56; 22.82$, respectively. Significant changes in the position, intensity, and appearance of new crystalline peaks in chitosan films after filling with NC-Ag bio-nanocomposites can indicate the ability of dispersed NC-Ag bio-nanocomposites to reflect its own diffraction peaks in the XRD pattern of chitosan. This was in contrast to what was found in previous works

when chitosan matrix was mixed with NC alone [13, 14, 53]. Moreover, the very low content of AgNPs, compared to the main components, cannot display its crystalline peaks clearly because it can be easily overcome by the semi-crystalline pattern of chitosan polymer.

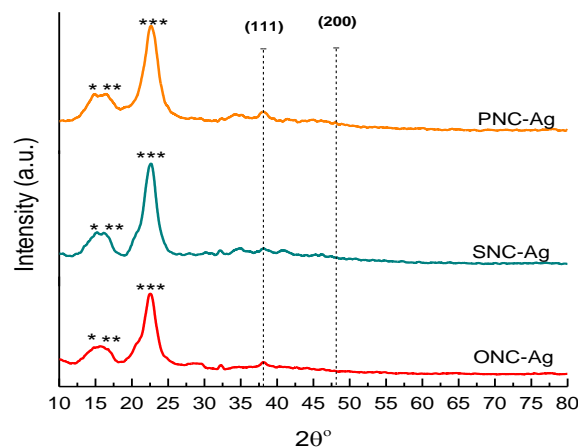


Fig. 5 XRD patterns [* , ** & *** refer to (110), (111), and (200) lattice planes of NC, respectively].

3.6. Antimicrobial test

At present, AgNPs are classified as an antimicrobial agent with a wide spectrum. Hence, implementations of AgNPs overcome classical borders and extended to new domains of interest such as clothing, pharmaceutical, cosmetics, and luxury [54]. In view of this, the suspensions of NC-Ag bio-nanocomposites prepared in this study, at dilution of 1:20, were tested against four bacterial species; *Bacillus subtilis*, *Staphylococcus aureus*, *Escherichia coli* and *Pseudomonas aeruginosa*. The disk-diffusion agar method demonstrated various microbial inhibition regions by NC-Ag bio-nanocomposites against the four bacterial organisms (Fig. 7). Even with low concentration, the biological activity of NCs showed significant enhancement after binding to Ag ions against all microorganisms of the test under study.

This improvement in activity indicates that this binding process can facilitate the ability of biogenic AgNPs to cross the cell membrane. This binding can also improve the lipophilic character of Ag atoms, which then prefers to penetrate through the lipid layer of the cell membrane causing interference with normal cell processes [55, 56]. The difference in the efficacy of the antibacterial activity of each NC-Ag bio-nanocomposites in the test can be attributed to the differences in the electrostatic interaction between the functional groups of NC and AgNPs, which depend on the chemical content, structure, and charge of the polymer [57].

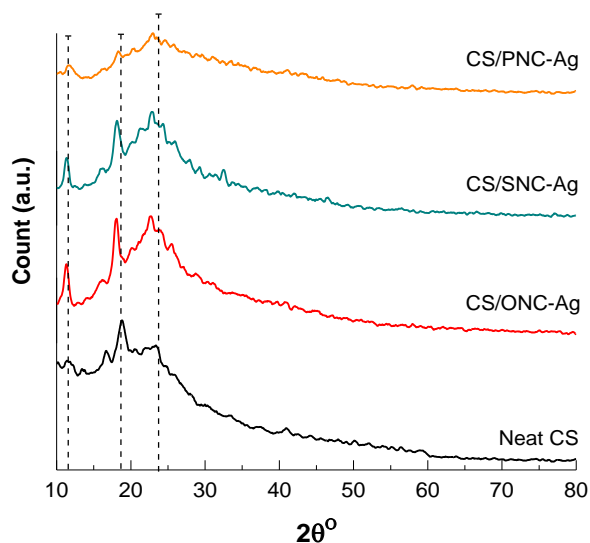


Fig. 6 XRD pattern of neat chitosan and chitosan films loaded with ONC-Ag, SNC-Ag, and PNC-Ag bio-nanocomposites.

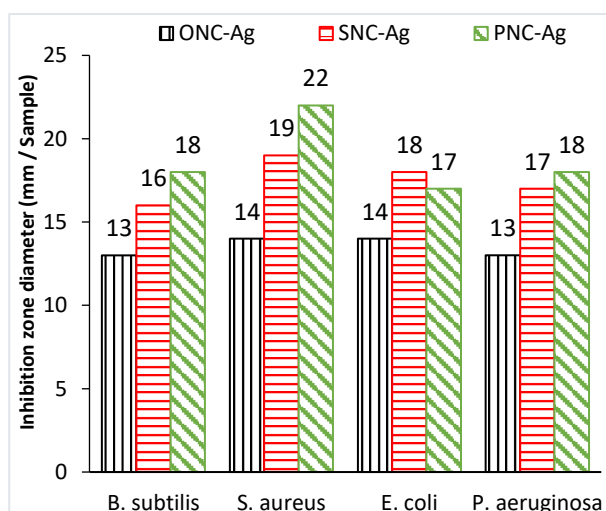


Fig. 7 Antimicrobial activities of ONC-Ag, SNC-Ag, and PNC-Ag bio-nanocomposites using the disk-diffusion agar method.

Antimicrobial examinations of the prepared films were achieved in quantitative and qualitative terms. Qualitative test was performed by means of disk-diffusion agar method, while quantitative test was performed by detecting percentage growth inhibition. The results of both the qualitative and quantitative testing are presented in Fig. 8. When explaining the results, it is also important to consider the dependence of the shape and size of the clear zone in the disk-diffusion agar procedure primarily on the contact area, the type of solid medium, the size of the inoculum and the ratio of the disk area. As can be seen from Fig. 8 (a), the antimicrobial activity of all tested films against the four microorganisms was reliant on the film used. The neat chitosan film did not show clear areas for inhibition of microbes, while

CS/SNC-Ag and CS/PNC-Ag bio-nanocomposite films showed distinct microbial inhibition regions against the four microorganisms under testing. Though chitosan itself is well known for its ability to inhibit microbial growth due to cationic amino groups, the apparently adverse result of neat chitosan film is mostly because of the limitations of detecting antimicrobial activity when applying the disk-diffusion agar procedure [58]. Of particular note, CS/ONC-Ag film inhibited only the growth of *Staphylococcus aureus* and *Escherichia coli*.

The quantitative test was performed on chitosan films, i.e. viable cell colony count procedure, to affirm the results from the qualitative antimicrobial test (Fig. 8 (b and c)). Like the results from the disk-diffusion agar method, the chitosan films' ability to inhibit microbial growth varies reliant on the microorganisms and films tested. Neat chitosan and chitosan bio-nanocomposite films have displayed antimicrobial activity against Gram-positive bacteria (i.e. *Bacillus subtilis* and *Staphylococcus aureus*). The antimicrobial activity of the neat chitosan film can attribute to the combined influence of chitosan and organic acid solvent (i.e. acetic acid), while the improved antimicrobial activity of films incorporated with NC-Ag bio-nanocomposites can credit to Ag high infiltration and high bactericidal activity. The Ag ions are reported to adhere to the negatively charged wall of the bacterial cells, thereby altering the permeability of the cell wall. This procedure, along with protein denaturation, leads to cell degradation and decease. The antimicrobial activity of Ag ion is also associated with its capacity to alter the mechanisms of DNA replica plus causing distortions in cell membranes, cytoplasmic contents, size and outer cell layers of sensitive cells [58, 59]. The whole evaluation of microbial reduction ratios in the current work disclosed that Gram-negative bacteria and *Aspergillusniger* fungi are more liable to the antimicrobial influence of Ag ions than Gram-positive bacteria and yeast (*Candida albicans*), and it is assumed that this attributed to the thinner cell wall, which may permit faster inclusion of ions inside the cell [53].

The only exception is CS/PNC-Ag bio-nanocomposite film that exhibits improved antimicrobial activity against Gram-positive bacterium, *Bacillus subtilis*.

3.7. Physicomechanical analysis of chitosan bio-nanocomposite films

The surface microstructures of neat chitosan and chitosan bio-nanocomposite films are displayed in Fig. 9. All the chitosan films have uniform thickness without any pores, cracks and macroscopic bubbles. The superficial form of the neat chitosan film was smooth and homogenous.

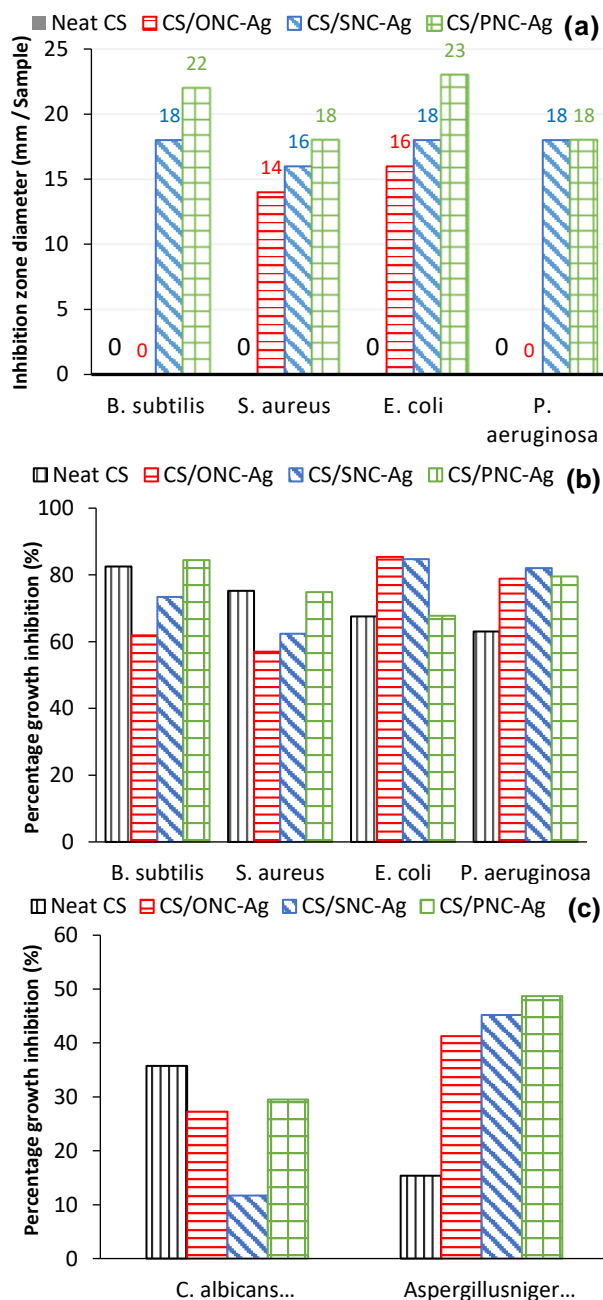


Fig. 8 Antimicrobial activities of neat chitosan and chitosan bio-nanocomposite films using (a) disk-diffusion agar method and (b & c) viable cell colony count method.

After adding NC-Ag bio-nanocomposites, the homogeneity and smoothness of the film's surface were reduced. However, the NC-Ag bio-nanocomposites are fully dispersed in the chitosan matrix with insignificant fragments or crumbs that likely assemble on the surface of the films.

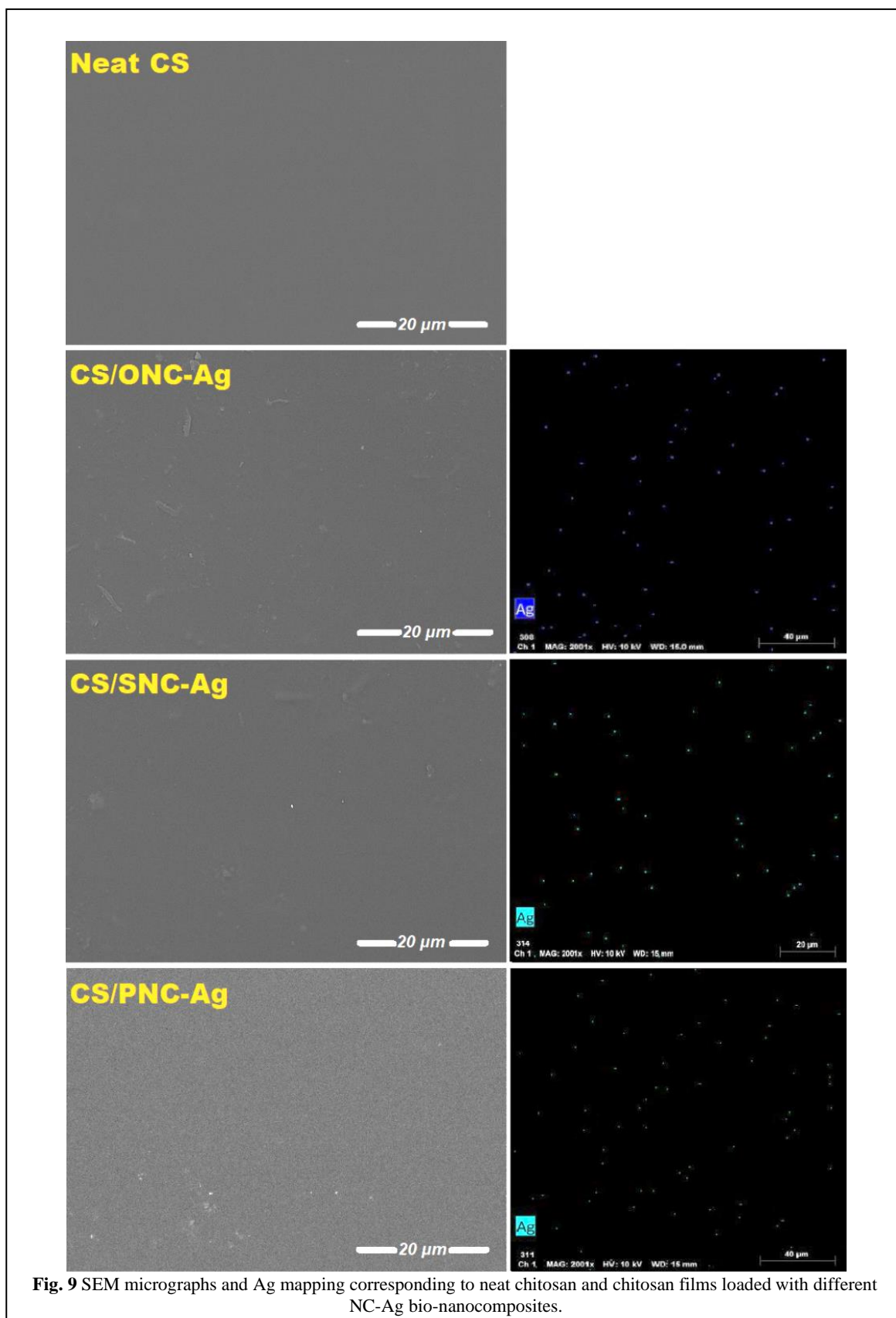
As can be seen from elemental analysis of the film's surface (Fig. 10), the presence of AgNPs with a very faint content in the tested films can be attributed to the low concentration of ONC-Ag, SNC-Ag, and

PNC-Ag in the chitosan bio-nanocomposite matrices (Fig. 9).

WVP is an essential physical feature of packaging, protective coating and other applications requiring effective polymer barriers [60]. As can be seen from Table 3, the WVP values for films with different NC-Ag bio-nanocomposites are different. WVP for neat chitosan film decreased significantly by 22% and 15% when loaded with SNC-Ag and PNC-Ag bio-nanocomposites, respectively. This finding is consistent with what Fortunati and co-workers found when they studied the barrier properties of films based on poly (lactic acid) filled with NC-Ag bio-nanocomposites [61]. The WVP weakness can be attributed to the NC which is believed to enhance the tortuosity in chitosan films resulting in slower diffusion of water vapor, and thus to reduce permeability [62]. On the contrary, the WVP for CS/ONC-Ag bio-nanocomposites film has not changed.

Table 3 shows the data obtained from the tensile test of neat chitosan and chitosan bio-nanocomposite films. The neat chitosan film exhibits a stress, strain and YM of 15.48 MPa, 77.99% and 41.33 MPa, respectively, while chitosan bio-nanocomposite films display stress of 18.05, 23.68 and 29.69 MPa after adding 7% of ONC-Ag, SNC-Ag and PNC-Ag bio-nanocomposites, respectively. The mechanical strength of the neat chitosan film, at maximum load, was influenced by the addition of NC-Ag bio-nanocomposites. Likewise, all chitosan bio-nanocomposite films showed an improvement in the YM parameter. YM increased by \approx 139.12, 183.09 and 86.67% with ONC-Ag, SNC-Ag and PNC-Ag bio-nanocomposites, respectively. As previously concluded from FTIR analysis, these new observed values of stress and YM for chitosan bio-nanocomposite films compared to the neat chitosan film suggest the formation of more bonds between the chains of chitosan and NC-Ag bio-nanocomposites in the bio-nanocomposite film. These bonds enhance the network structure and allow stress transfer from chitosan matrix to NC fibers, thereby raise the tensile strength of CS/NC-Ag bio-nanocomposite films. These results are analogous to what was found by other researchers who studied chitosan bio-nanocomposite films [53, 63].

In addition, the color intensity of films varied depending on the type of NC-Ag bio-nanocomposites. Therefore, the neat chitosan film is transparent and slightly yellowish, while chitosan bio-nanocomposite films range in color from golden yellow to reddish-brown (Online resource 2).



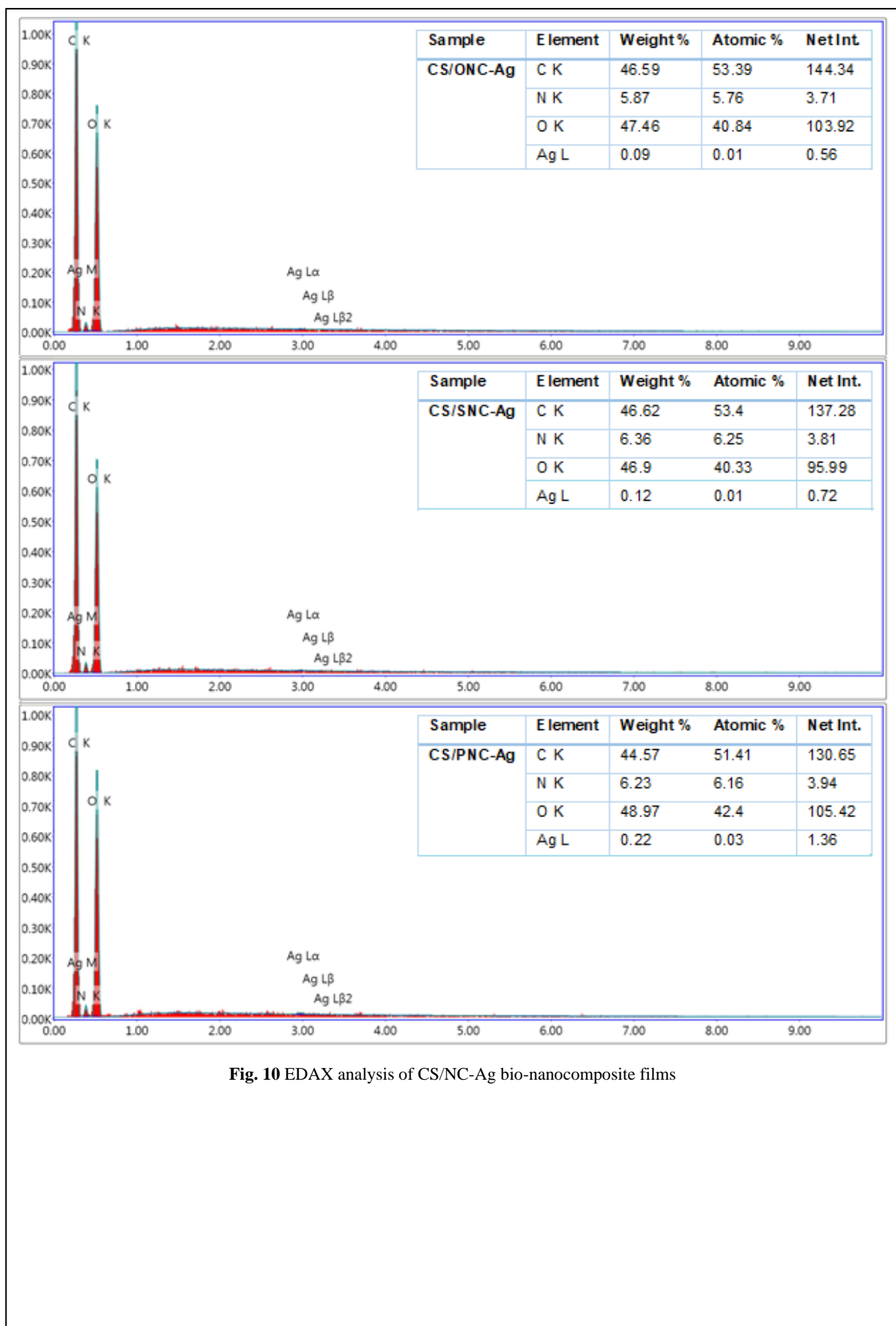


Fig. 10 EDAX analysis of CS/NC-Ag bio-nanocomposite films

Table 2 FTIR absorption band assignments and hydrogen bonding interactions (R & EH) for of NCs and NC-Ag bio-nanocomposites

Band assignment	Band position (cm ⁻¹)						References
	ONC	ONC-Ag	SNC	SNC-Ag	PNC	PNC-Ag	
-OH stretching inter and intra-molecular hydrogen bonds	3401	3420	3417	3419	3414	3425	[39]
CH stretching, CH ₂ asymmetric stretching	2906	2903	2913	2920	2910	2923	[40]
C=O stretching vibration of COOH groups	1727	--	--	--	--	--	[41, 42]
H-O-H bending and stretching vibration	1636	1618	1643	1631	1633	1632	[43]
CH ₂ symmetric scissoring of pyran ring, OH plane deformation vibration	1435	1427	1451	1425	1440	--	[44]
CH symmetric bending, CH deformation vibration or CH ₂ vibration	1383	1372	1384	1381	1378	1390	[28, 44]
CH ₂ wagging	1329	1320	1330	1320	1329	1321	[45]
CH bending	1239	1240	1274	1277	--	--	[46]
C-O-C stretching from the glucosidic units	1161	1163	1163	1160	1158	1157	[47]
Ring asymmetric stretching, C-C & C-O stretching	1109	1113	1111	1111	1106	1115	[48]
β-(1→4)- glucosidic linkage	1060	1062	1053	1054	1047	1049	[49]
C-H out of plane in position in ring stretching in cellulose due to β-linkage	902	901	884	896	897	897	[49]
Ag-O stretching vibration	--	561, 521	--	565, 525	--	564, 522	[38]
R (nm)	2.784	2.788	2.788	2.788	2.787	2.789	[13]
EH (kcal)	4.266	3.936	3.986	3.969	4.035	3.837	[13]

Table 3 WVP, mechanical and XRD parameters of neat chitosan and chitosan bio-nanocomposite films

Parameters	Neat CS	CS/ONC-Ag	CS/SNC-Ag	CS/PNC-Ag
WVP (10 ⁻³ .g/m.day.kPa)	2.67±0.08	2.67±0.19	2.09±0.07	2.28±0.22
Stress (MPa)	15.48±1.71	18.05±1.50	23.63±1.83	29.69±2.15
Strain (%)	77.99±5.31	54.04±7.67	64.96±6.34	99.02±10.67
YM (MPa)	41.33±5.60	98.83±12.64	117.00±16.51	77.15±7.30
Position-2θ (°)	--	11.29	11.33	11.56
	16.76	16.35	16.07	16.25
	19.10	18.10	18.13	18.21
	--	22.66	22.83	22.82
d-spacing (Å)	--	7.84	7.81	7.66
	5.29	5.42	5.51	5.45
	4.64	4.90	4.89	4.87
	--	3.92	3.10	3.89

4. Conclusions

In the present study, NCs with different ionic content, particle size and number of electron pairs were utilized to afford products with precise characteristics required for the fabrication of ONC-Ag, SNC-Ag, and PNC-Ag bio-nanocomposites. Next, an active packaging material was developed by incorporation of NC-Ag bio-nanocomposites into the chitosan matrix. Based on the results obtained, we can draw the following conclusions.

- The presence of plasmon peak distinctive for AgNPs at about 408 nm with a PWHM range between 83.38 to 128.80 nm confirms the formation of pseudo-spherical AgNPs.

Also, measurements of UV-Vis absorption spectra over a long period of storage indicate that all suspensions of the prepared ONC-Ag, SNC-Ag, and PNC-Ag bio-nanocomposites are stable for more than 5 months.

- ONC-Ag, SNC-Ag, and PNC-Ag bio-nanocomposites, according to this study, can be classified as broad-spectrum antibacterial agents. Thus it qualifies for potential application in new consumer products such as multi-purpose antimicrobial coatings, ordinary antiseptic sprays and sanitizing soaps.

- From analyses tools of SEM, XRD, and EDAX, Ag present with a faint content in the tested films.
 - Data obtained from the qualitative test of the disk-diffusion agar method for the chitosan bio-nanocomposite films indicate that these substances belong to a wide range of antimicrobial agents. Also, the quantitative test using a viable cell colony count method reveals that *Aspergillusniger* fungi and Gram-negative bacteria are more susceptible to the microbicidal effect of CS/NC-Ag than Gram-positive bacteria and *Candida albicans* yeast.
 - Based on these improvements in tensile strength, water vapor barrier and microbicidal efficacy, these active films of CS/NC-Ag bio-nanocomposite can be considered a sustainable candidate for various industrial applications such as active packaging.
 - Finally, different functionalized NCs in NC-Ag bio-nanocomposites demonstrate different permanence, antimicrobial and biocompatibility efficiency.
- 5. Conflicts of interest**
There are no conflicts to declare.
- 6. Funding sources**
Partial financial support was received from National Research Centre, Egypt.
- 7. Acknowledgments**
The authors appreciate the kind assistance of Dr. Muhammad Al-Awadi, Department of Microbial Biotechnology, in conducting quantitative antimicrobial testing.
- 8. References**
1. Marchioni M, Jouneau P-H, Chevallet M, et al (2018) Silver nanoparticle fate in mammals: Bridging in vitro and in vivo studies. *Coord Chem Rev* 364:118–136. <https://doi.org/10.1016/j.ccr.2018.03.008>
 2. Quadros ME, Marr LC (2011) Silver nanoparticles and total aerosols emitted by nanotechnology-related consumer spray products. *Environ Sci Technol* 45:10713–10719. <https://doi.org/10.1021/es202770m>
 3. Hasan A, Waibhaw G, Saxena V, Pandey LM (2018) Nano-biocomposite scaffolds of chitosan, carboxymethyl cellulose and silver nanoparticle modified cellulose nanowhiskers for bone tissue engineering applications. *Int J Biol Macromol* 111:923–934. <https://doi.org/10.1016/j.ijbiomac.2018.01.089>
 4. Carbone M, Donia DT, Sabbatella G, Antiochia R (2016) Silver nanoparticles in polymeric matrices for fresh food packaging. *J King Saud Univ - Sci* 28:273–279. <https://doi.org/10.1016/j.jksus.2016.05.004>
 5. Adel AM, Al-Shemy MT, Diab MA, et al (2021) Fabrication of packaging paper sheets decorated with alginate/oxidized nanocellulose-silver nanoparticles bio-nanocomposite. *Int J Biol Macromol* 181:612–620. <https://doi.org/10.1016/j.ijbiomac.2021.03.182>
 6. González AL, Noguez C, Beránek J, Barnard AS (2014) Size, shape, stability, and color of plasmonic silver nanoparticles. *J Phys Chem C* 118:9128–9136. <https://doi.org/10.1021/jp5018168>
 7. Fahmy Y, Tamer YA Fahmy, Fardous Mobarak, et al (2017) Agricultural residues (wastes) for manufacture of paper, board, and miscellaneous products: Background overview and future prospects." Fahmy Y, Fahmy TYA, Mobarak F, El-Sakhawy M, Fadl MH (2017) Agricultural Residues (Wastes) for Manufacture of Paper, Board, and Miscellaneous Products: Background Overview and Future Prospects. *Int J ChemTech Res* 10:424–448
 8. Fahmy TYA, Fahmy Y, Mobarak F, et al (2020) Biomass pyrolysis: past, present, and future. *Environ Dev Sustain* 22:17–32. <https://doi.org/10.1007/s10668-018-0200-5>
 9. Mohamed SO, El-Naggar K, Khalil MMH (2022) Green Synthesis of Silver Nanoparticles using Egyptian Propolis extract and its Antimicrobial Activity. *Egypt J Chem* 65:453–464. <https://doi.org/10.21608/ejchem.2021.104296.4838>
 10. Yamal G, Sharmila P, Rao KS, Pardha-Saradhi P (2013) Inbuilt Potential of YEM Medium and Its Constituents to Generate Ag/Ag₂O Nanoparticles. *PLoS One* 8:e61750. <https://doi.org/10.1371/journal.pone.0061750>
 11. Eissa D, Hegab RH, Abou-Shady A, Kotp YH (2022) Green synthesis of ZnO, MgO and SiO₂ nanoparticles and its effect on irrigation water, soil properties, and *Origanum majorana* productivity. *Sci Rep* 12:.. <https://doi.org/10.1038/s41598-022-09423-2>
 12. Biliuta G, Coseri S (2019) Cellulose: A ubiquitous platform for ecofriendly metal nanoparticles preparation. *Coord Chem Rev* 383:155–173. <https://doi.org/10.1016/j.ccr.2019.01.007>
 13. Adel AM, El-Shafei AM, Ibrahim AA, Al-Shemy MT (2019) Chitosan/Nanocrystalline Cellulose Biocomposites Based on Date Palm (*Phoenix Dactylifera* L.) Sheath Fibers. *J Renew Mater* 7:567–582.

- <https://doi.org/10.32604/jrm.2019.00034>
14. Adel AM, El-Shafei A, Ibrahim A, Al-Shemy M (2018) Extraction of oxidized nanocellulose from date palm (*Phoenix Dactylifera* L.) sheath fibers: Influence of CI and CII polymorphs on the properties of chitosan/bionanocomposite films. *Ind Crops Prod* 124:155–165. <https://doi.org/10.1016/j.indcrop.2018.07.073>
 15. Adel AM, El-Shafei A, Al-Shemy M, et al (2017) Influence of cellulose polymorphism on tunable mechanical and barrier properties of chitosan/oxidized nanocellulose bio-composites. *Egypt J Chem* 60:639–652. <https://doi.org/10.21608/ejchem.2017.1194.1062>
 16. Halib N, Perrone F, Cemazar M, et al (2017) Potential applications of nanocellulose-containing materials in the biomedical field. *Materials (Basel)* 10:1–31. <https://doi.org/10.3390/ma10080977>
 17. Fortunati E, Armentano I, Zhou Q, et al (2012) Multifunctional bionanocomposite films of poly(lactic acid), cellulose nanocrystals and silver nanoparticles. *Carbohydr Polym* 87:1596–1605. <https://doi.org/10.1016/j.carbpol.2011.09.066>
 18. Feng J, Shi Q, Li W, et al (2014) Antimicrobial activity of silver nanoparticles in situ growth on TEMPO-mediated oxidized bacterial cellulose. *Cellulose* 21:4557–4567. <https://doi.org/10.1007/s10570-014-0449-2>
 19. Romainor ANB, Chin SF, Pang SC, Bilung LM (2014) Preparation and characterization of chitosan nanoparticles-doped cellulose films with antimicrobial property. *J Nanomater* 2014:. <https://doi.org/10.1155/2014/710459>
 20. Caschera D, Toro RG, Federici F, et al (2020) Green approach for the fabrication of silver-oxidized cellulose nanocomposite with antibacterial properties. *Cellulose* 27:8059–8073. <https://doi.org/10.1007/s10570-020-03364-7>
 21. El-Shafei AM, Adel AM, Ibrahim AA, Al-Shemy MT (2019) Dual functional jute fabric biocomposite with chitosan and phosphorylated nano-cellulose (antimicrobial and thermal stability). *Int J Biol Macromol* 124:733–741. <https://doi.org/10.1016/j.ijbiomac.2018.11.137>
 22. Battisti R, Fronza N, Vargas Júnior Á, et al (2017) Gelatin-coated paper with antimicrobial and antioxidant effect for beef packaging. *Food Packag Shelf Life* 11:115–124. <https://doi.org/10.1016/j.fpsl.2017.01.009>
 23. Parreidt TS, Müller K, Schmid M (2018) Alginate-Based Edible Films and Coatings for Food Packaging Applications. *Foods* 7:170. <https://doi.org/10.3390/foods7100170>
 24. Adel AM, Ibrahim AA, El-Shafei AM, Al-Shemy MT (2019) Inclusion complex of clove oil with chitosan/ β -cyclodextrin citrate/oxidized nanocellulose biocomposite for active food packaging. *Food Packag Shelf Life* 20:100307. <https://doi.org/10.1016/j.fpsl.2019.100307>
 25. Bourtoom T, Chinnan MS (2008) Preparation and properties of rice starch-chitosan blend biodegradable film. *LWT - Food Sci Technol* 41:1633–1641. <https://doi.org/10.1016/j.lwt.2007.10.014>
 26. Da Silva JBA, Nascimento T, Costa LAS, et al (2015) Effect of Source and Interaction with Nanocellulose Cassava Starch, Glycerol and the Properties of Films Bionanocomposites. *Mater Today Proc* 2:200–207. <https://doi.org/10.1016/j.matpr.2015.04.022>
 27. Adel A, El-Shafei A, Ibrahim A, Al-Shemy M (2018) Extraction of oxidized nanocellulose from date palm (*Phoenix Dactylifera* L.) sheath fibers: Influence of CI and CII polymorphs on the properties of chitosan/bionanocomposite films. *Ind Crops Prod* 124:155–165. <https://doi.org/10.1016/j.indcrop.2018.07.073>
 28. Adel AM, Abd El-Wahab ZH, Ibrahim AA, Al-Shemy MT (2011) Characterization of microcrystalline cellulose prepared from lignocellulosic materials. Part II: Physicochemical properties. *Carbohydr Polym* 83:676–687. <https://doi.org/10.1016/j.carbpol.2010.08.039>
 29. Al-shemy MT, Al-sayed A, Dacrory S (2022) Fabrication of sodium alginate / graphene oxide / nanocrystalline cellulose scaffold for methylene blue adsorption: Kinetics and thermodynamics study. *Sep Purif Technol* 290:120825. <https://doi.org/10.1016/j.seppur.2022.120825>
 30. CLSI (2016) Performance Standards for Antimicrobial Susceptibility Testing. 26th ed. CLSI supplement M100S
 31. Kalembe D, Kunicka A (2003) Antibacterial and Antifungal Properties of Essential Oils. *Curr Med Chem* 10:813–829. <https://doi.org/10.2174/0929867033457719>
 32. Lokanathan AR, Uddin KMA, Rojas OJ, Laine J (2014) Cellulose nanocrystal-mediated synthesis of silver nanoparticles: Role of sulfate groups in nucleation phenomena. *Biomacromolecules* 15:373–379. <https://doi.org/10.1021/bm401613h>
 33. El-Sheikh MA (2022) A Novel Photosynthesis of Carboxymethyl Starch-Stabilized Silver Nanoparticles: Experimental Investigation. *Innov Sci Technol Vol* 4 69–83. <https://doi.org/10.9734/bpi/ist/v4/7463d>
 34. Hebeish A, El-Shafei A, Sharaf S, Zaghloul S (2011) Novel precursors for green synthesis and application of silver nanoparticles in the realm of cotton finishing. *Carbohydr Polym* 84:605–613.

- <https://doi.org/10.1016/j.carbpol.2010.12.032>
35. Liu L, Liang X, Qiu G, et al (2022) Self-Assembly Silver Nanoparticles Decorated on Gold Nanoislands for Label-Free Localized Surface Plasmon Resonance Biosensing. *Adv Mater Interfaces* 9:1–12. <https://doi.org/10.1002/admi.202200339>
36. Adrianto N, Panre AM, Istiqomah NI, et al (2022) Nano-Structures & Nano-Objects Localized surface plasmon resonance properties of green synthesized silver nanoparticles. *Nano-Structures & Nano-Objects* 31:100895. <https://doi.org/10.1016/j.nanoso.2022.100895>
37. Laudenslager MJ, Schiffman JD, Schauer CL (2008) Carboxymethyl Chitosan as a Matrix Material for Platinum, Gold, and Silver Nanoparticles. *Biomacromolecules* 9:2682–2685. <https://doi.org/10.1021/bm800835e>
38. Teli MD, Sheikh J (2013) Study of grafted silver nanoparticle containing durable antibacterial bamboo rayon. *Cellul Chem Technol* 47:69–75
39. Kumar A, Lee Y, Kim D, et al (2017) Effect of crosslinking functionality on microstructure, mechanical properties, and in vitro cytocompatibility of cellulose nanocrystals reinforced poly (vinyl alcohol)/sodium alginate hybrid scaffolds. *Int J Biol Macromol* 95:962–973. <https://doi.org/10.1016/j.ijbiomac.2016.10.085>
40. Taher FA, Moselhy WA, Mohamed AF, et al (2017) Preparation and Characterization of Shrimp Derived Chitosan and Evaluation of Its Efficiency As Bee Venom Delivery for Cancer Treatment. *Int J Adv Res* 5:370–388. <https://doi.org/10.21474/IJAR01/4122>
41. Tan C, Peng J, Lin W, et al (2015) Role of surface modification and mechanical orientation on property enhancement of cellulose nanocrystals/polymer nanocomposites. *Eur Polym J* 62:186–197. <https://doi.org/10.1016/j.eurpolymj.2014.11.033>
42. Rosli NA, Ahmad I, Abdullah I (2013) Isolation and characterization of cellulose nanocrystals from agave angustifolia fibre. *BioResources* 8:1893–1908. <https://doi.org/10.15376/biores.8.2.1893-1908>
43. El-Sakhawy M, Adel AM, Diab MA, Al-Shemy M (2020) Facile methods for the preparation of micro- and mesoporous amorphous silica from rice husk. *Biomass Convers Biorefinery* 1–10. <https://doi.org/10.1007/s13399-020-01112-2>
44. Adel AM, El-Wahab ZHA, Ibrahim AA, Al-Shemy MT (2010) Characterization of microcrystalline cellulose prepared from lignocellulosic materials. Part I. Acid catalyzed hydrolysis. *Bioresour Technol* 101:4446–4455. <https://doi.org/10.1016/j.biortech.2010.01.047>
45. Sen S, Singh A, Kailasam K (2022) Nanoscale Advances oxide-based nanohybrids for thermal insulation. <https://doi.org/10.1039/d2na00010e>
46. Kathiresan S, Meenakshisundaram O (2022) Effect of alkali treated and untreated cellulose fibers and human hair on FTIR and tensile properties for composite material applications. *SN Appl Sci* 4:. <https://doi.org/10.1007/s42452-022-04946-9>
47. Saad F, Hassabo A, Othman H, et al (2022) A valuable observation on thickeners for valuable utilisation in the printing of different textile fabrics. *Egypt J Chem* 65:1–2
48. Mohi MA, Ismail S, others (2022) Assessment of the applicability of cellulolytic enzyme in disassembling of caked papers. *Egypt J Chem* 65:1–2
49. El-Shafei AM, Adel AM, Ibrahim AA, Al-Shemy MT (2019) Dual functional jute fabric biocomposite with chitosan and phosphorylated nano-cellulose (antimicrobial and thermal stability). *Int J Biol Macromol* 124:733–741. <https://doi.org/10.1016/j.ijbiomac.2018.11.137>
50. Anicuta S, Dobre L, Stroescu M, Jipa I (2010) Fourier transform infrared (ftir) spectroscopy for characterization of antimicrobial films containing chitosan. *Analele Univ din Oradea Fasc Ecotoxicologie, Zooteh si Tehnol Ind Aliment* 1234–1240
51. Segal L, Creely JJ, Jr. AEM, Conrad CM (1959) An Empirical Method for Estimating the Degree of Crystallinity of Native Cellulose Using the X-Ray Diffractometer. *Text Res J* 29:786–794. <https://doi.org/10.1177/004051755902901003>
52. Patterson AL (1939) The Scherrer Formula for X-Ray Particle Size Determination. *Phys Rev* 56:978–982. <https://doi.org/10.1103/PhysRev.56.978>
53. Rhim JW, Hong SI, Park HM, Ng PKW (2006) Preparation and characterisation of chitosan-based nanocomposite films with antimicrobial activity. *J Agric Food Chem* 54:5814–5822
54. Betiha MA, Kheiralla ZM, Mansour AS, et al (2022) A Review on Different Plants Extract Mediated Silver Nanoparticles: Preparation, Antimicrobials, and Antioxidant. *Egypt J Chem* 65:575–589. <https://doi.org/10.21608/ejchem.2021.99747.4637>
55. Ibrahim AA, Adel AM, El-Wahab ZHA, Al-Shemy MT (2011) Utilization of carboxymethyl cellulose based on bean hulls as chelating agent. Synthesis, characterization and biological activity. *Carbohydr Polym* 83:94–115. <https://doi.org/10.1016/j.carbpol.2010.07.026>
56. Abd El-Wahab ZH, Faheim AA (2009) Metal

- complexes of phosphorus compounds including indigoid structure: synthesis, characterization, and biological study. *Phosphorus, Sulfur, and Silicon* 184:341–361
57. Eli Rohaeti, Endang Widjajanti LFX and AR (2014) Silver Nanoparticle Impregnated on the Composite of Bacterial Cellulose-Chitosan-Glycerol As Antibacterial. 18–20
58. Malinowska-Pańczyk E, Staroszczyk H, Gottfried K, et al (2015) Antimicrobial properties of chitosan solutions, chitosan films and gelatin-chitosan films. *Polimery/Polymers* 60:735–741. <https://doi.org/10.14314/polimery.2015.735>
59. Hebeish A, El-Shafei A, Sharaf S, Zaghoul S (2014) Development of improved nanosilver-based antibacterial textiles via synthesis of versatile chemically modified cotton fabrics. *Carbohydr Polym* 113:455–462. <https://doi.org/10.1016/j.carbpol.2014.06.015>
60. Siracusa V (2012) Food Packaging Permeability Behaviour: A Report. *Int J Polym Sci* 2012:1–11. <https://doi.org/10.1155/2012/302029>
61. Fortunati E, Peltzer M, Armentano I, et al (2013) Combined effects of cellulose nanocrystals and silver nanoparticles on the barrier and migration properties of PLA nano-biocomposites. *J Food Eng* 118:117–124. <https://doi.org/10.1016/j.jfoodeng.2013.03.025>
62. Sanchez-Garcia MD, Gimenez E, Lagaron JM (2008) Morphology and barrier properties of nanobiocomposites of poly(3-hydroxybutyrate) and layered silicates. *J Appl Polym Sci* 108:2787–2801. <https://doi.org/10.1002/app.27622>
63. Yoksan R, Chirachanchai S (2010) Silver nanoparticle-loaded chitosan–starch based films: Fabrication and evaluation of tensile, barrier and antimicrobial properties. *Mater Sci Eng C* 30:891–897. <https://doi.org/10.1016/j.msec.2010.04.004>